#695

METEOSAT
ENERGETIC ELECTRON DETECTOR

88-051A-04A

METEOSAT

ENERGETIC ELECTRON DETECTOR

88-051A-04A

THIS DATA SET CATALOG CONSISTS OF 1 TAPE. THE TAPE IS A 9-TRACK,
6250 BPI, BINARY, LABELLED AND CREATED ON A VAX COMPUTER. THE D AND
C NUMBERS AND TIME SPANS ARE AS FOLLOWS:

D#	C#	FILES*	TIME SPANS
D-80282	C-27620	90	06/22/88 - 08/31/89

*30 DATA FILES. THE REST ARE HEADER AND TRAILER FILES.

MULLARD SPACE SCIENCE LABORATORY
DEPARTMENT OF PHYSICS AND ASTRONOMY
UNIVERSITY COLLEGE LONDON

Holmbury St. Mary

Dorking

Surrey

RH5 6NT

Tel (0483) 274111

Telex 859185 UCMSSL G

Fax (0483) 278312

January 25, 1990

Dr Joe King,
Code 633,
National Space Science Data Center,
NASA/Goddard Space Flight Center,
Greenbelt,
Maryland 20771,
USA

Dear Dr King,

ESA have agreed that we can send you the Meteosat SEM-2 data. I enclose a tape we have produced which includes fluxes covering the period June 88-Aug 89, together with documentation on how to read the tape. I hope you can read it successfully.

We are still processing the data and will be pleased to send you more in the Fall.

Yours sincerely,

Dr A.J. Coates

The tapes will consist of files of the form:

(1)   JUN89_ARCHIVE_HR.DAT - This contains the high resolution data.
(2)   JUN89_ARCHIVE_LR.DAT - This contains the low resolution data.

Each of these 2 files will be written for each month of Meteosat P2 data,
by the program [MAB.METEOSAT.P2]ARCHIVE_METEOSAT_P2.EXE, and the input
to this program is the disk file produced by H.E.Huckle's programs:
MONTH3_P2.EXE, MONTH2_P2.EXE on [HEH.METEOSAT.P2].

The files will be written to disk using the following open and write statements.
All variables are real*4 .

```
        open( unit        = lun_high,
    &         name        = archive_file(1),
    &         status      = 'new',
    &         access      = 'direct',
    &         recl        = 96,
    &         form        = 'unformatted',
    &         recordtype  = 'fixed' )

      do i = 1, num_hr_values
        !
        !               WRITE THE DATA TO THE HIGH RESOLUTION ARCHIVE FILE.
        !               ----------------------------------------------------
        !
        write( lun_high' i )
    &                   xb_hr(i),
    &                   xt_hr(i),
    &                   total_flux_hr(i),
    &                   y_e10_hr(i),
    &                   y_e21_hr(i),
    &                   y_e32_hr(i),
    &                   y_e43_hr(i),
    &                   y_e54_hr(i),
    &                   spectral_index_hr(i),
    &                   delta_spectral_hr(i),
    &                 ( polar_flow_hr(j,i), j = 1, 5),
    &                 ( azim_flow_hr(iaz,i), iaz = 0, 5),
    &               ( ( polar_azim_flux_hr(k,j,i), k = 0, 5 ), j = 1, 5 ),
    &                   c_e10_hr(i),
    &                   c_e21_hr(i),
    &                   c_e32_hr(i),
    &                   c_e43_hr(i),
    &                   c_e54_hr(i),
    &               ( ( polar_azim_counts_hr(k,j,i), k = 0, 5 ), j = 1, 5 ),
    &                   anistropy_hr(i),
    &                   thetapole_hr(i),
    &                   phipole_hr(i),
    &                   kpno_hr(i),
    &                   kpvalue_hr(i),
    &                   latch_hr(i),
    &                 ( zone_hr(k,i), k = 1, 4 )

      enddo

      close( unit = lun_high )

      open( unit        = lun_low,
```

```
     &            status     - 'new',
     &            access     - 'direct',
     &            recl       - 96,
     &            form       - 'unformatted',
     &            recordtype - 'fixed' )

        do i - 1, num_lr_values
          !
          !                 WRITE THE DATA TO THE LOW RESOLUTION ARCHIVE FILE.
          !                 - - - - - - - - - - - - - - - - - - - - - - - - - - - - - - - - - - - - - -
          !
          write( lun_low' i, iostat - iok )
     &                    xb_lr(i),
     &                    xt_lr(i),
     &                    total_flux_lr(i),
     &                    y_e10_lr(i),
     &                    y_e21_lr(i),
     &                    y_e32_lr(i),
     &                    y_e43_lr(i),
     &                    y_e54_lr(i),
     &                    spectral_index_lr(i),
     &                    delta_spectral_lr(i),
     &                  ( polar_flow_lr(j,i), j - 1, 5),
     &                  ( azim_flow_lr(iaz,i), iaz - 0, 5),
     &                ( ( polar_azim_flux_lr(k,j,i), k - 0, 5 ), j - 1, 5 ),
     &                    c_e10_lr(i),
     &                    c_e21_lr(i),
     &                    c_e32_lr(i),
     &                    c_e43_lr(i),
     &                    c_e54_lr(i),
     &                ( ( polar_azim_counts_lr(k,j,i), k - 0, 5 ), j - 1, 5 ),
     &                    anistropy_lr(i),
     &                    thetapole_lr(i),
     &                    phipole_lr(i),
     &                    kpno_lr(i),
     &                    kpvalue_lr(i),
     &                    latch_lr(i),
     &                  ( zone_lr(k,i), k - 1, 4 )

        enddo

        close( unit - lun_low )
```

These items being the following:

Monthly High Time Resolution Files
- -

These will have time resolution of 500, 500 and 600 seconds. The parameters
to be included are:

Start Time	(1)
End Time	(1)
Total Flux	(1)
Flux(E)	(5)
Spectral Index	(1)
Error Bar of Spectrum	(1)
Polar Flow	(5)
Azimuthal Flow	(6)
Polar-Azim Flux	(5,6)
Counts(E)	(5)
Polar-Azim Counts	(5,6)
Anistropy	(1)

```
theta                      (1)
phi                        (1)
Kp                         (1)
Kp(tau)                    (1)
MUM                        (5)  recognize startup pattern and
                                set to zero before adding
```

Monthly Low Time Resolution Files

These will have time resolution of 30 minutes. The parameters to be included
are the same as the high time resolution files. Except for the MUM which is a
sum. All the others are averages:

The data contains 48 thirty minute bins per day, with the first bin starting at
midnight. If any of these periods contains no data all the data values are
set to -1's.

```
Start Time                 (1)
End Time                   (1)
Total Flux                 (1)
Flux(E)                    (5)
Spectral Index             (1)  average distribution before calculating
Error Bar of Spectrum      (1)
Polar Flow                 (5)
Azimuthal Flow             (6)
Polar-Azim Flux            (5,6)
Counts(E)                  (5)
Polar-Azim Counts          (5,6)
Anisotropy                 (1)  average result after calculating
theta                      (1)         "
phi                        (1)         "
Kp                         (1)
Kp(tau)                    (1)
MUM                        (5)  recognize startup pattern and
                                set to zero before adding
```

All the files will then simply copied to tape, using the following commands:

```
$!
$ allocate mfa0:
$ ini      mfa0: metp2 / dens - 6250 / override - owner_identifier
$ mount    mfa0: metp2 / dens - 6250 / override - owner_identifier
$ copy *.* mfa0:[]*.*
$ dismount mfa0:
$ dealloc  mfa0:
$!
```

Quest for the source of Meteosat anomalies

A.J.Coates, A.D.Johnstone, D.J.Rodgers

Mullard Space Science Laboratory, University College London,

Holmbury St Mary, Dorking, Surrey RH5 6NT, UK

G.L.Wrenn, A.J.Sims

Space Departmentt, Royal Aerospace Establishment,

Farnborough, Hants GU14 6TD, UK

Abstract

Three ESA Meteosat geostationary satellites have suffered from a series of anomalies which disturb routine operations; most commonly, the scan of the radiometer has stopped or jumped requiring a reset command to be sent.

Experience with Meteosat-F1 launched in 1977 (Robbins, 1979) prompted the installation of an AFGL electron spectrometer (50eV-20keV) on Meteosat-F2, in an attempt to demonstrate a direct link between the anomalies and surface charging. Data spanning August 1981 to March 1987 have provided interesting evidence for differential charging (Wrenn and Johnstone, 1987) and permit the establishment of an empirical model of charging fluxes through a solar cycle. However, the reported anomalies do not fit the pattern for surface charging effects and no real link was found. Deep dielectric charging has now become the most likely explanation and consequently Meteosat-P2, launched in June 1988, carries a LANL monitor of 43-300 keV electrons.

The Meteosat anomaly chronicle is the result of reliable recording procedures at ESOC and it represents a unique data base for an important class of ESD effects which occur at Geosynchronous orbit. This paper gives some preliminary results from Meteosat P2 and attemptes to assess their relevance within the context of earlier conclusions from the Meteosat-F2 studies.

INTRODUCTION

Since Meteosat-F1 suffered many operational anomalies it was decided to include a spacecraft charging monitor on F2 to see whether the anomalies were related to spacecraft surface charging. While that experiment certainly showed strong evidence of charging on F2 there was no correlation with the occurence of unexplained anomalies, which were also present on F2. The decision was then made to investigate the higher energy range of electrons associated with deep dielectric charging. Thus SEM-2 was commissioned to study the 30-300keV range of electrons.

The sensor unit was provided by Los Alamos National Laboratory, USA as a spare Lo-E sensor [Aiello et al, 1975] from other programmes, to the Mullard Space Science Laboratory of University College London (MSSL) which provided the power supplies, data processing unit and interface to the Meteosat spacecraft. MSSL was further responsible for integration, testing and calibration of the instrument, and delivery of the instrument to the spacecraft. MSSL also provided a memory upset monitor (MUM) in this instrument, as requested by ESA.

This paper describes briefly the history of the F1 and F2 studies, in particular the role of spacecraft charging in generating the anomalies and the possibility of deep dielectric charging as an explanation. We then go on to a description of the SEM-2 instrument, and the conversion of the observed counts to physical units. Typical natural events in the spacecraft environment as seen by SEM-2 are shown. The correlation of the energetic electron fluxes to the occurence of anomalies, which on P2 occur at a rate which is about four times that of F2, are the major results. As data have accumulated we have been able to show a striking correlation between the energetic electron fluxes and the spacecraft anomalies. For the first time it appears that the measurements provide a good indication of anomalies.

1 Meteosat operational anomalies and spacecraft charging

1.1 Meteosat-F1

When Meteosat-F1 was launched in 1977 many operational anomalies occurred (about 150 in 3 years) for which there was no immediate explanation. However, their occurrence was related to geophysical factors outside the normal realm of spacecraft engineering, namely that they were more likely when there was strong geomagnetic

1979]. It had recently been discovered then that geosynchronous spacecraft could charge up to many thousands of Volts [deForest, 1972] in the ambient plasma so it was natural to attribute the anomalies to charging, or more precisely to differential charging. Unless the complete outer surface of the spacecraft is conductive and electrically connected, it is normal for different parts of the spacecraft to charge to different voltages. At times, adjacent surfaces can be more than a thousand volts apart. This in turn leads to arcing between the surfaces and results in large electrical transients in the spacecraft harness. After the problems were encountered by Meteosat-F1 a series of laboratory tests was carried out which demonstrated that arcing occurred if the spacecraft was illuminated by an electron beam, and that electrical transients could induce anomalous behaviour. It was not possible to simulate in-orbit conditions completely and thus it was not possible to establish the causal chain completely.

1.2 Meteosat-F2

Before the second spacecraft Meteosat-F2 was launched some changes were made to reduce the susceptibility to differential charging, namely grounding of thermal shields and hardening of some critical electrical interfaces, and to include two charging monitors to complete the link between the anomalies and spacecraft charging. One of the monitors was designed to detect arcing transients on a short antenna within the spacecraft. In flight no such events were detected, but it is not known whether the instrument was sensitive enough, or whether it was not operating correctly or whether there were no significant transients. Therefore we can say no more about it. The second monitor measured the ambient plasma electrons in the energy range 50eV to 20KeV and therefore could measure the charging current directly. Not only that but it was anticipated that in the event of spacecraft charging the energy spectrum would be modified in a manner which would allow the spacecraft potential to be measured. Briefly, the objective of the instrument was to see if the anomalies occurred when the spacecraft was charged. The results of this investigation have been published in a number of reports [Johnstone et al, 1985, Wrenn and Johnstone, 1987]. Although no direct link between differential charging and anomalies was found there were several interesting and significant (for this problem) findings which we summarize here.

1. Two types of differential charging were observed. One type occurred during eclipses and had been expected. The second type, called a "barrier event", only occurred when the radiometer mirror was completely in shadow and was therefore probably because the mirror was charging up. The two types are illustrated in Figures 1 and 2 and explained in the figure captions.

2. A charging index based on an estimate of the net electron flux to the spacecraft (incident electrons minus secondary emitted electrons) was 95 percent successful in predicting whether the spacecraft would charge up in any particular eclipse.

3. There was an indication in the electron spectrum during eclipse charging that the voltages in differential charging were limited by discharging currents of secondary electrons from one part of the spacecraft to another.

4. Only one anomaly, in more than 100, occurred at any time near an observable differential charging event. In all cases there was no evidence that the spacecraft was charged to more than a few volts.

5. The anomalies attributed for lack of a better cause to arcing did, as before on Meteosat-F1, show a dependence on geophysical parameters, ie local time, solar aspect angle and geomagnetic activity [see Figure 3].

6. When separated into four types of anomaly the solar aspect angle, and local time dependence was different for all four groups.

7. The most common type of anomaly, the radiometer stoppage or position jump was most common at the equinox and was associated with a period of sustained high geomagnetic activity.

The conclusions of the analysis were that the anomalies were not the result of differential charging but that they were caused by some external geophysical effect. The four types of anomaly were caused by four different mechanisms.

Frezet et al [1989] have made an analysis of the charging of Meteosat with the NASCAP charging analysis code. They find that the differential voltages developed are greater at equinox and suggest that this is the explanation for the occurrence of radiometer anomalies at this time. The charging levels they obtain are many thousands of volts. However the only differential charging of the radiometer is observed away from equinox, when the radiometer mirror is totally in shadow. Also

4

developed such a charging scenario when extreme plasma conditions are used and such extreme conditions were not observed by the monitors on Meteosat-F2 itself.

We were left with the situation that we still do not know what caused the anomalies on Meteosat-F1 or F2. Spacecraft surface charging, or differential charging, appears to be ruled out. In their final report Johnstone et al [1985] suggested that it might be caused by penetrating electrons producing deep dielectric charging. This was partly based on the observation that a sustained period of high geomagnetic activity was required to develop the effect, and that the trapped energetic electrons are known to be slower to respond to geomagnetic activity than the plasma at energies of less than 20KeV. Therefore it was suggested that the third Meteosat flight should carry a detector of more energetic electrons. Accordingly it was decided to include in the payload the SEM-2 detector which measures the energy and angular distribution of electrons in the energy range 30KeV to 300KeV.

The behaviour of electrons above 30keV at Geosynchronous orbit has been studied by the Los Alamos group [Baker et al, 1981]. In Figure 4 the average fluxes for the whole of 1977 and 1978 are compared to the particles' range in aluminium as calculated by the SHIELDOSE program: this shows that higher energy particles can penetrate appreciable distances before being stopped. To penetrate 0.5mm into polythene, an electron requires an energy of 200KeV (see Figure 5 from Powers et al. [1981]). Deep dielectric charging, where penetrating electron fluxes may cause buildup of charge and eventual breakdown in insulators, has been postulated as the reason for anomalies on other spacecraft [eg Baker et al, 1986].

2 Instrumentation

The measurement of electrons above 30 keV implies a different type of sensor to the F2 instrument, which consisted of two electrostatic energy analyser/channeltron combinations, giving differential energy measurements. The standard technique for tens to hundreds of keV particles has become the surface barrier solid-state detector [eg Aiello et al, 1975]. Using electronic thresholds this technique also gives differential energy measurements.

SEM-2 contains five surface barrier detector-collimator systems, arranged to accept particles from 5 different angular ranges. The 5 ranges are of spacecraft polar angle: azimuthal angle measurements are achieved by timing. Each of the detectors

... ... energy acceptances were found by calibr... ...n at the Goddard spaceflight center and are as follows:

Energy level	E_{min} (keV)
E5	42.9
E4	59.4
E3	90.7
E2	134.9
E1	201.8

Table 1: Lower level discriminator settings for SEM-2

Full details of the operation of the instrument are given in the final report to ESA (Coates et al, 1989). Here we restrict ourselves to a description of the information transmitted.

A transmission list is accumulated in 4 formats, approx 100 seconds. A complete experiment cycle takes 500 or 600 seconds since one polar angle is sampled in each 4-format cycle. The raw parameters received on the ground are as follows, every 100 seconds.

- A 5-point energy spectrum, compressed counts E1-E5, for a particular polar angle, summed over azimuth.

- A 6-point azimuth array, compressed counts A1-A6, for a particular polar angle, summed over energy.

- Overflow information as appropriate for each of the above bins.

- Timing information to relate azimuth to spin phase.

- Synchronisation information for data checking.

- MUM parameters on SEU and latch-up.

Counts are converted to flux and plotted. The principal result of the data processing was the provision of summary plots of the data from SEM-2. It is essential that users of the SEM-2 data be able to tell from the plots alone, the general behaviour of the plasma environment at all times and be able to identify times of particular interest. To enable this, the plots contain parameters that summarise the data, parameters that interpret the data further and associated parameters for comparison. This led to the choice of eight panels of data presented on a single page with one page per day; an example is shown in Figure 6. These panels are:

and axis of symmetry; Kp; MUM and Latch-up.

2.1 Total Flux

Total flux of electrons within the energy range of the detector (42.9-300keV) and summed over all polar and azimuthal bins.

2.2 Flux

This is the Flux (expressed as a grey scale level) in the 5 energy bands of the analyser, from 43 to 300KeV. These energy bands are: 42.9 to 59.4KeV, 59.4 to 90.7KeV, 90.7 to 134.9KeV, 134.9 to 201.8KeV, 201.8 to 300(nominal)KeV. These data are summed over all polar and azimuthal angle bins.

The analyser returns integral measurements of counts versus energy. Counts are measured as the energy cut-off or threshold of the instrument is progressively raised. To calculate the counts in one energy band, the counts measured with the cut-off at the top and bottom of that band are subtracted.

2.3 Spectral Index

This index determines the 'hardness', or shape of the energy spectrum. This is generally negative because, except in extraordinary cases, there are less particles at high energy than at low energy. The index is simply the slope of the log of the energy spectrum.

2.4 Polar Flow

This is the flux (expressed as a grey scale) in the 5 polar angle sectors of the analyser. These sectors look in the polar directions 30°, 60°, 90°, 120° and 150° to the spacecraft spin axis. The spacecraft spin axis is to a good approximation parallel to the Earth's spin axis. The angle bins cover a nominal ±5°.

2.5 Azimuthal Flow

This is the flux (expressed as a grey scale) in the 6 azimuthal angle sectors of the analyser. These sectors cover the angles 0° to 60°, 60° to 120°, 120° to 180° , 180° to 240°, 240° to 300° and 300° to 360°, in spacecraft coordinates. Note that at 0° the analyser looks towards the sun.

The anisotropy index describes the angular shape of the plasma distribution relative to its axis of symmetry, shown as theta and phi. A trapped particle distribution is a 'pancaked' i.e. enhanced perpendicular to the magnetic field compared to along it. Where plasma is newly injected it tends to lie along the field line in a 'cigar-shaped' distribution. The index is positive for pancaked distributions and negative for cigar-shaped distributions. The anisotropy index is calculated [using techniques adapted from Sanderson and Page, 1974, Sanderson and Hynds, 1977, Higbie and Moomey, 1977] by fitting the data to a set of spherical harmonics. Since we believe that the magnetic field organizes the plasma, then the axis of symmetry represents the magnetic field direction. However, it does not distinguish between positive and negative field directions.

2.7 Kp and Kp(τ)

Kp is an index of planetary magnetospheric activity for the whole of Earth, in a three hour period. In the monthly plots, Kp(τ) is plotted. This is a weighted average of successive Kp values and was devised by Wrenn [1987]. Many magnetospheric processes are more dependent on the general level of magnetospheric activity in the recent past than on the present level. Wrenn showed that anomalies on Meteosat-F2 was better correlated with an appropriately time-averaged activity index than with the real-time index.

2.8 MUM

The Memory Upset Monitor results are displayed as lines in the bottom panel. These display the number of 'single-event upsets' i.e. errors found in a known memory pattern, in the 4 memory zones of the test RAM. A test pattern is seen in the plot when the instrument is first powered on. A fifth line in this plot shows the occurrence of 'Latch-ups' where the test RAM attempts to draw excessive current. This line can take only values 1 – Latch-up and 0 – no latch-up.

3 Typical events

To illustrate the environment at Geosynchronous orbit as seen by Meteosat P2 SEM-2 we include some data examples.

27th June 88 (Figure 6): On the dayside, eg at 1300Z, a "pancake" distribution is seen in the polar angle plot where fluxes are peaked at the equator: this is typical for a trapped electron distribution diffusing into the loss cone. At approximately 0200Z there is a typical isolated, injection event which shows some important features. First the total flux drops by two orders of magnitude, relatively slowly. Then it increases sharply to a level greater than before. Finally it decreases slowly to the initial level.

In Figure 7 we have looked at the results from 4 satellites simultaneously to the injection in Figure 6. Local time around the Earth is seen in the small inset diagram; spacecraft 1 and 2 (Meteosat) see the injection, while 3 and 4 show velocity dispersion with higher energy electrons arriving first.

The monthly summary example in Figure 8 shows the wider view of the dramatic events during March 1989. The spacecraft was outside the magnetopause for significant times on March 13 since the magnetosphere was severely compressed at that time.

4   Meteosat anomaly correlations

When comparing the occurrence of anomalies with the results from SEM-2 on a monthly basis it soon became apparent that anomalies, particularly radiometer anomalies, nearly always occurred when the flux of energetic electrons was high. The problem then becomes to verify such an association statistically and then to try and determine a causal link. While we have been able to achieve the former, the latter is still some way from a satisfactory conclusion. In other words there is no doubt that anomalies and high energetic electron fluxes are linked but we do not yet know if the energetic electrons cause anomalies and if they do, how they do. Alternatively the high electron fluxes may themselves be the consequence of another agent which is the actual cause of the anomalies.

A plot of the anomalies we have used in this study is given in Figure 9, where we have organized the anomalies as follows:

RPJ   Radiometer position jump
RDS   Radiometer stoppage
RGC   Radiometer gain change
BAT   Battery anomaly
SIC   SIC anomaly
OTH   Other anomaly

RDS is by far the most frequent type of anomaly.

First we establish that the radiometer anomalies show the same systematic behaviour as on the previous Meteosat flight models. Figure 9 shows the local time and annual distribution for the 76 unexplained anomalies seen in the first year. They are essentially identical with distributions obtained for F2. In local time the peak occurrence is in the period 02 to 05 local time but there is a non-negligible rate of occurrence throughout the day. This distribution is reminiscent of the distribution of a type of charging event on Meteosat-F2 which were called barrier events [Johnstone et al, 1985]. However none of the Meteosat-F2 anomalies was concurrent with a barrier event. Anomalies are, as with F2, are most likely at the equinoxes and least likely at the solstices. This demonstrates once again essentially a dependence on solar aspect angle. The main conclusion we wish to draw from this diagram is that the radiometer anomalies are caused by the same mechanism as on Meteosat-F2. It is interesting to note that the anomaly rate is approximately 4 times that of F2, which suffered 80 anomalies in 4 years.

In the next series of plots the statistics of the average daily flux is examined. Figure 10 is a histogram of the number of days in the year a particular value of the daily average flux was recorded. For example the column labelled 7 contains number of days the average fluxes were in the range 7000 to 7999. Thus this graph if normalized would show the probability that the average flux has a particular value. It could be used for example to calculate the amount of radiation a geosynchronous satellite would encounter. Figure 11 shows the yearly total number of anomalies which occurred on days with that average daily flux. Compared with the distribution of Figure 10 it is clearly strongly biased towards the higher fluxes. By dividing the distribution of Figure 11 by that in Figure 10 we calculate the average number of anomalies in a day if the average flux has the given value. This produces the very striking distribution shown in Figure 12. Once the flux exceeds 19000 the average daily rate is greater than one. This can be interpreted as the probability of an anomaly in given flux conditions. It is the first time we have achieved a connection between a characteristic of the plasma environment and the occurrence of anomalies. No such connection was found between the low energy plasma (E < 20 KeV) environment and anomalies on Meteosat-F2.

This does not yet establish a causal connection because the high fluxes $\cap$ $\dashv$ be caused by the same unknown phenomenon which causes the anomaly. W out the annual variation in the occurrence? This could arise because th tic

electron fluxes have a similar annual variation. In Figure 5 the mean monthly flux (dotted line) is plotted with the monthly number of anomalies. Both show a peak in March and April which were two of the most active months magnetically for a long time. In Sept and Oct where the anomaly rate peaks the monthly mean flux actually has its minimum value for the year. This suggests that there are at least two independent factors responsible for radiometer anomalies; one is associated with high fluxes of energetic electrons fluxes, and the other with the solar aspect angle.

It is possible that there is a third factor, which we see in the form of the local time variation of anomalies. This is likely however to be linked to a local time variation in the energetic electron fluxes. We have not been able to test this hypothesis yet because of the need to develop some specialised software to access this aspect of the data.

These results give us a positive result on the cause of anomalies for the first time. It is difficult to achieve a better level of proof without having a clearer idea of the mechanism which will allow us to develop a physical model which can be directly tested. An attempt to do this based on deep dielectric charging will form the next stage of our investigation.

The interaction between Meteosat and the environment is clearly a very complex one which we do not yet understand. Although spacecraft charging is significant, and needs to be minimized as we have now learned, there are other things going on for which we have not yet found the appropriate ameliorative methods.

Clearly the investigation should continue. Ideas of such effects as deep dielectric charging are still vague and need to be sharpened. This may require laboratory testing to try to replicate the phenomena, and the development of physical models which can be tested against the observations. There is also still a need to observe in more detail the interaction of a spacecraft with its environment and over a wide range of energies.

5 Summary of results

- Unexplained anomalies on Meteosat-P2 have continued at a rate about 4 times higher than that observed on F2. The P2 and F2 anomalies show a similar local time and seasonal dependance.

- The anomalies show a good correlation with electron fluxes in the range 43-300keV. This is the first time that a correlation of anomalies has been demon-

11

strated with the Meteosat in-situ environment monitor data - the charging instrument on F2 saw charging events but they did not correlate with anomalies. Taken on its own the P2 correlation would confirm deep dielectric charging as a possible mechanism.

- However the seasonal dependence of anomalies, which strongly peak at equinox, show that at least one additional process is at work.

- We still maintain that spacecraft charging cannot explain the observed Meteosat anomalies, although it should still be minimised to avoid others.

6 Further study

Future study will be pursued on the following items:

- Processing of further SEM-2 data (already underway at MSSL).

- An explanation should be sought for the seasonal variation of anomalies on Meteosat.

- Further study is needed on the deep dielectric charging mechanism.

- Further effort should be put into calculating dose rates and penetration depths from the SEM-2 data.

- Further instruments should be included on future spacecraft, not only Meteosat, to look at both charging and deep dielectric effects. For the Meteosat series, higher energy electrons measurements extending up to 1MeV are encouraged to study the deep dielectric charging in more detail.

7 References

Aiello, W.P., Belian, R.D., Conner, J.P., Higbie, P.R., Martin, W.B. & Singer, S., "An energetic particle detector for a synchronous satellite", *IEEE Trans Nucl Sci*, **NS-22**, 575, 1975.

Baker, D.N., Belian, R.D., Higbie, P.R., Klebsbadel, R.W. and Blake, J.B., "Deep dielectric charging effects due to high energy electrons in Earth's outer magnetosphere", submitted to *J.Electrostatics*, 1986.

Baker, D.N., Higbie, P.R., Belian, R.D., Aiello, W.P., Hones, E.W.,Jr., Tech, E.R., Halbig, M.F., Payne, J.B., Robinson,R. and Kedge, S., "The Los Alamos Geostationary Orbit Synoptic Data Set: a compilation of energetic particle data", *Los Alamos report LA-8843*, 1981.

Coates, A.J., Johnstone, A.D., Rodgers, D.J and Huckle, H.E., "SEM-2 ,data processing 22 June 1988 to 30 June 1989", report on ESA contract 7879/88/F/TB, 1989.

DeForest, S.E., "Spacecraft charging at synchronous orbit", *J.Geophys.Res.*, **77**, p651, 1972.

Frezet, M., Daly, E.J., Granger, J.P and Hamelin, J., "Assessment of electrostatic charging of satellites in the geostationary environment", ESA Journal, **13**, 89-117, 1989.

Higbie P.R. and Moomey W.R. "Pitch Angle Measurements from Satellites Using Particle Telescopes with Multiple View Directions", *Nucl. Instrum Methods*, **146** p.439, 1977.

Johnstone A.D., Wrenn G.L., Huckle H.E. and Scott R.F. "Meteosat-F2 Spacecraft Charging Monitors", Final Report ESA contracts 4715/81/F/CG, 5911/84/F/CG, 1985.

Powers W.L., Adams B.F. and Inouye G.T. "Electron Penetration of Spacecraft Thermal Insulation", Spacecraft Charging Technology 1980, *AFGL-TR-81-0270*, p.86, 1981.

Robbins,A., "Meteosat spacecraft charging investigations", final report, ESA contract 3561/78F/CG/SC, 1979.

Sanderson T.R. and Hynds R.J. "Multiple Telescope Measurements of Particle Anisotropies in Space", *Planet. Space Sci.*, **25** p.799, 1977.

Sanderson T.R. and Page D.E. "Spherical Harmonic Analysis of Satellite Anisotropy Measurements", *Nucl. Instrum. Methods*, **119**, p.177, 1974.

Wrenn G.L., "Time-Weighted Accumulations ap(τ) and Kp(τ)", *J. Geophys. Res.*, **92**, no. A9, p.10125, 1987.

Wrenn, G.L. and Johnstone, A.D., "Evidence for differential charging on Meteosat-2", *J.Electrostatics*, **20**, 59-84, 1987.

Figure 1 - An eclipse charging event seen by the F2 experiment. From the change in the energy spectrum it is inferred that the potential of the whole satellite went 5kV negative relative to space in this eclipse. The rising peak is due to differential charging of another part of the spacecraft at an even more negative potential (up to 600V more negative). [from Johnstone et al, 1985].

Figure 2 - Example of a "barrier event" on F2. This is where part of the spacecraft, electrically isolated from the rest, is shadowed and charges negatively as the whole spacecraft does in eclipse. High potential differences between adjacent parts of the spacecraft may then result in arcing. The low energy electrons observed in the event are due to reflection by the potential barrier of photo- and secondary electrons back to the spacecraft. While these events were correlated with radiometer mirror shadowing they were not correlated with observed anomalies. [from Johnstone et al, 1985].

Figure 3 - Distribution of F2 anomalies in local time and season [from Wrenn, 1989].

Figure 4 - Average electron flux spectra averaged over the 2 years 1977 and 1978. 90% of the samples are below the top curve and above the bottom curve. Mean electron ranges are also plotted. [fluxes from Baker et al, 1981, range from SHIELDOSE code developed by Seltzer (NBS 1116)]

Figure 5 - Electron range in polyethylene [from Powers et al, 1981]

Figure 6 - Daily plot for 27 June 88 showing an injection event at 0220Z.

Figure 7 - Energetic electron measurements from various positions at Geosynchronous orbit around the earth (see inset), showing the 27 June injection on spacecraft 1 and 2 (Meteosat) and velocity dispersion effects on 3 and 4. 1,3,4 are US spacecraft, those data courtesy LANL.

Figure 8 - Monthly plot for March 89

Figure 9 - All P2 anomalies as a function of local time and date

Figure 10 - Number of days with given average flux (thousands of flux units)

Figure 11 - Anomalies as a function of daily flux

Figure 12 - Average daily anomaly rate (anomaly probability) as a function of daily flux

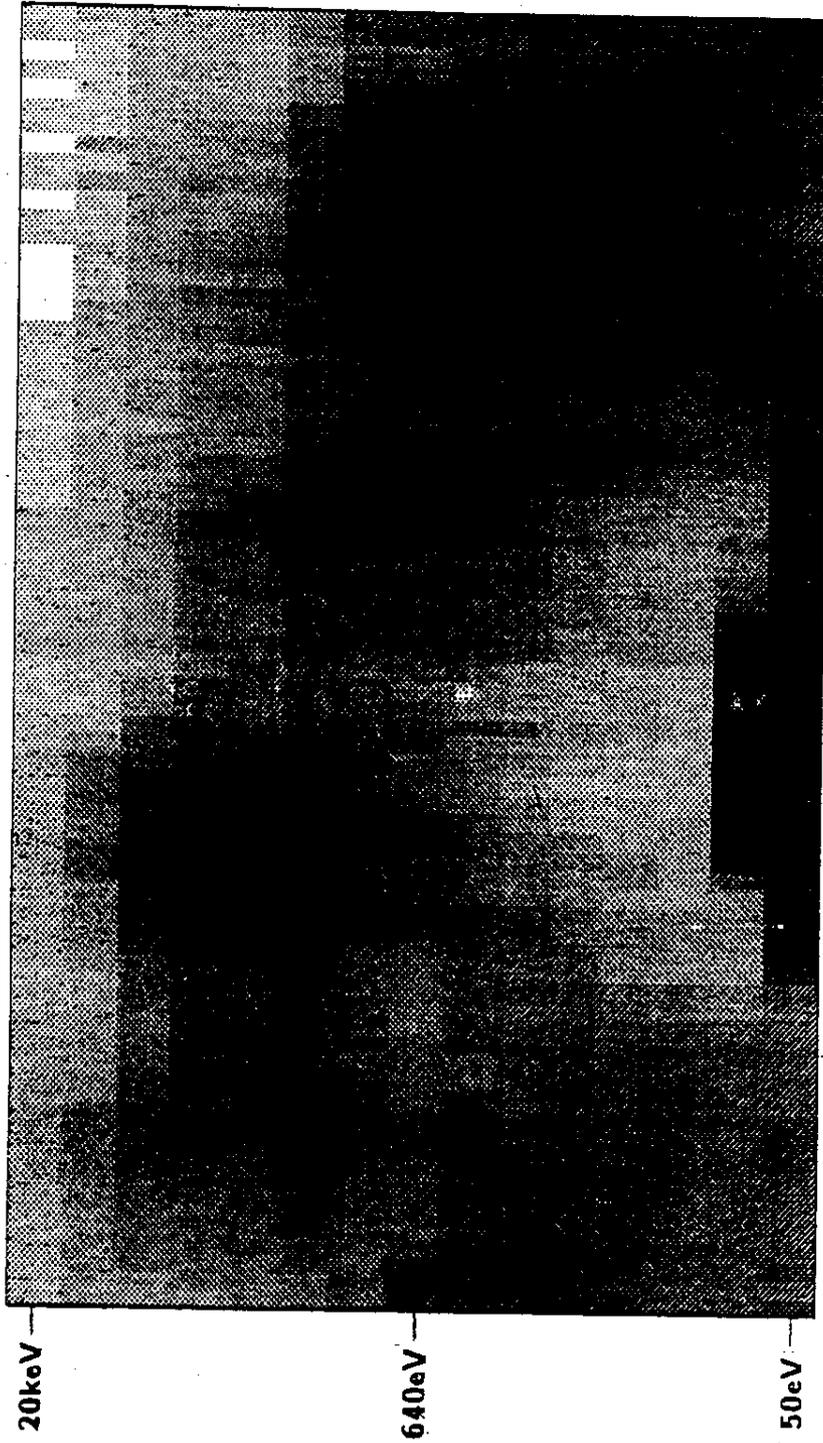Figure 13 - Anomalies (solid line) and monthly mean flux (dotted line for different months

Meteosat F2, SSJ/3 Data   3/4 April 1982

19·8 keV

640 eV

50 eV

2300

0100

U.T.

Eclipse
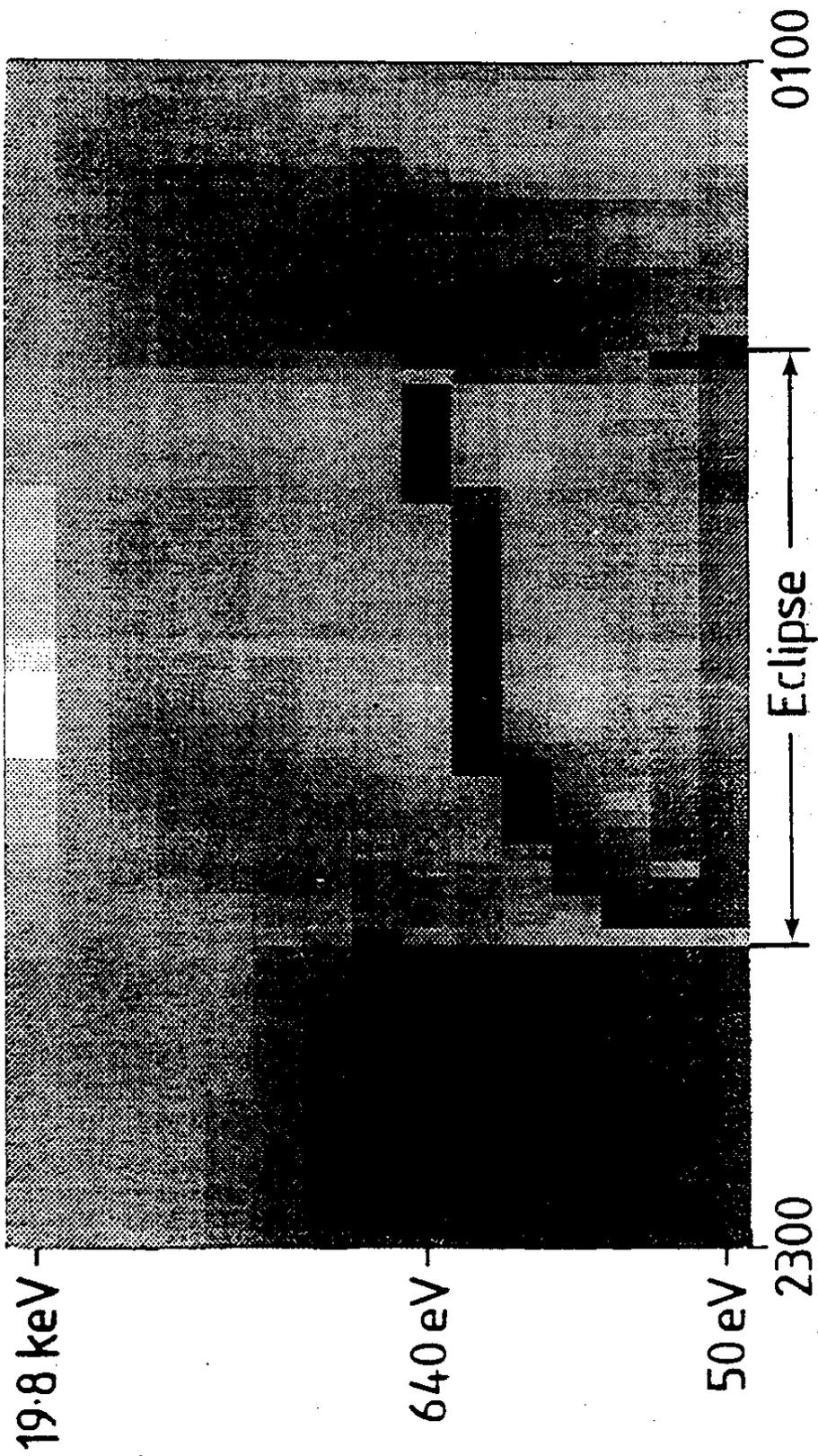
FIG 1

METEOSAT F2, SSJ/3 DATA
STARTING AT 3 1 41.8 ON 25/ 7/82

20keV —

640eV —

50eV —

← Barrier Event →

2 HOURS

FIG 2

METEOSAT ANOMALIES (1981-85)

LOCAL TIME (h)

METEOSAT-1   METEOSAT-2

RADIometer   ·   o
CALibration   □   □
Power SS/BAT o   x
AOCS/SIC   +
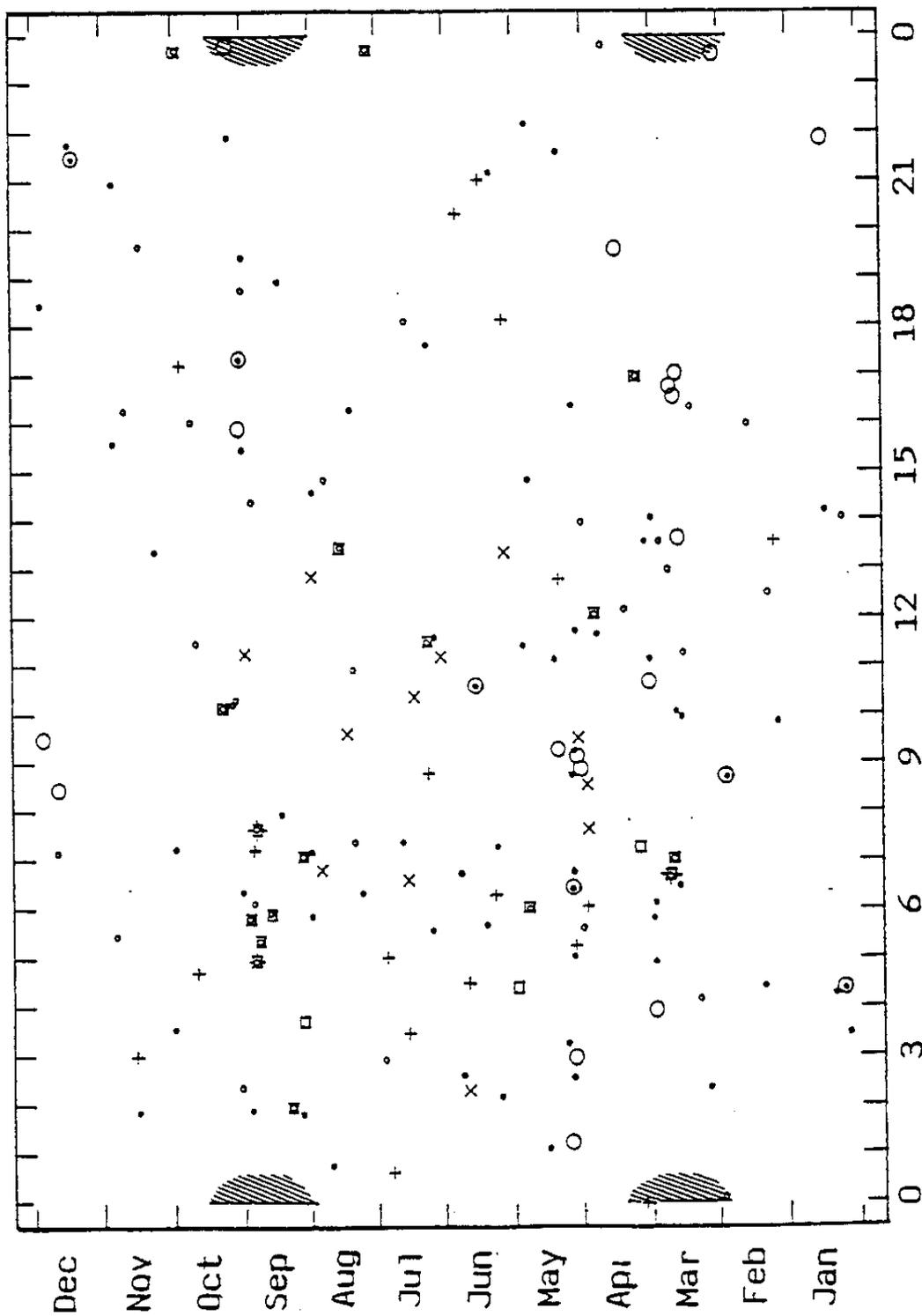
FIG 3

ENERGETIC ELECTRON FLUX and RANGE
ALL LOCAL TIMES, 1977 & 1978

Log [Flux (/cm² s sr keV)]

mm Al

6
5
4
3
2
1
0

ENERGY (keV)

10   100   1000

6
5
4
3
2
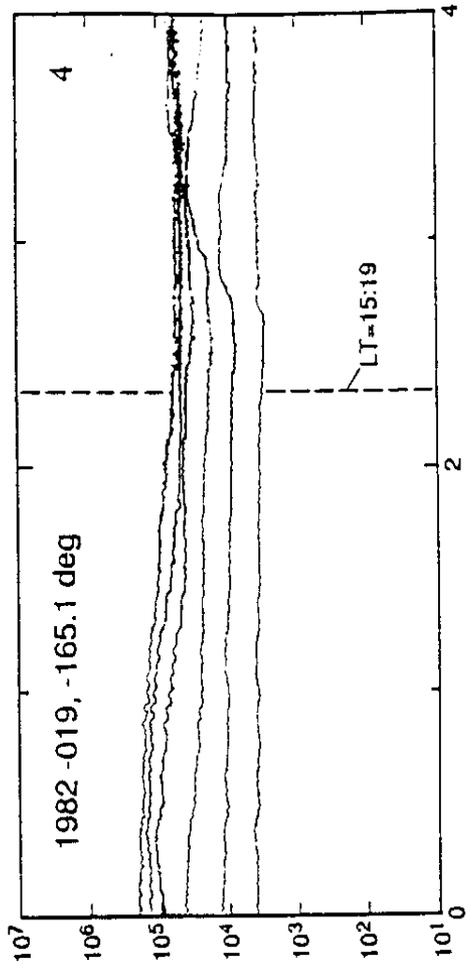1
0

FIG 4.

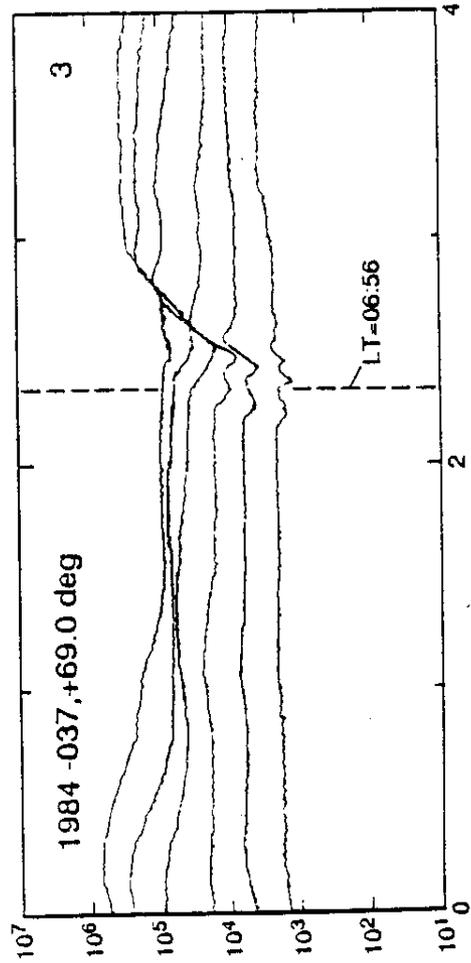——— 10%   ———*——— 50%   ———·——— 90%   ——— Range
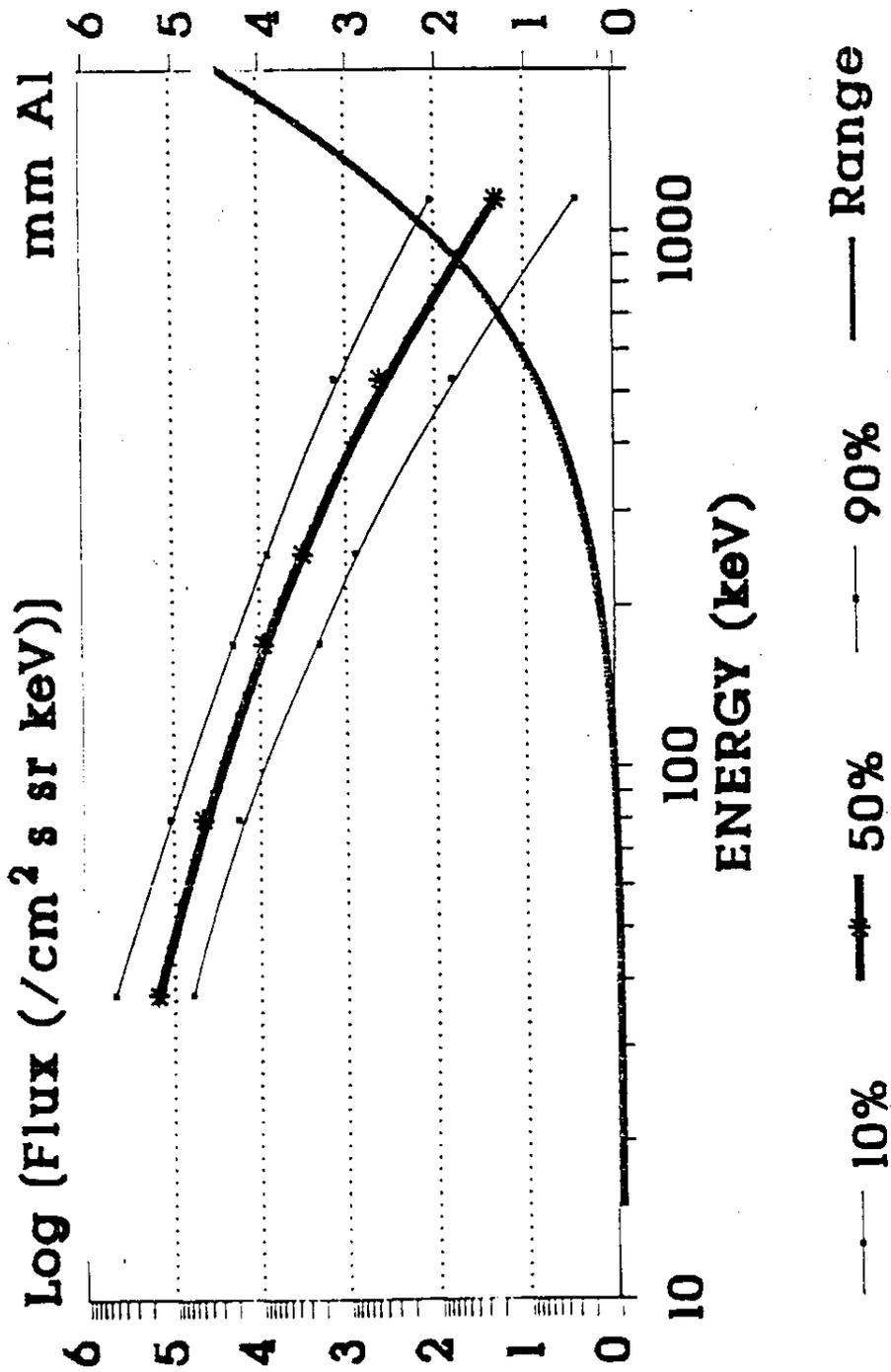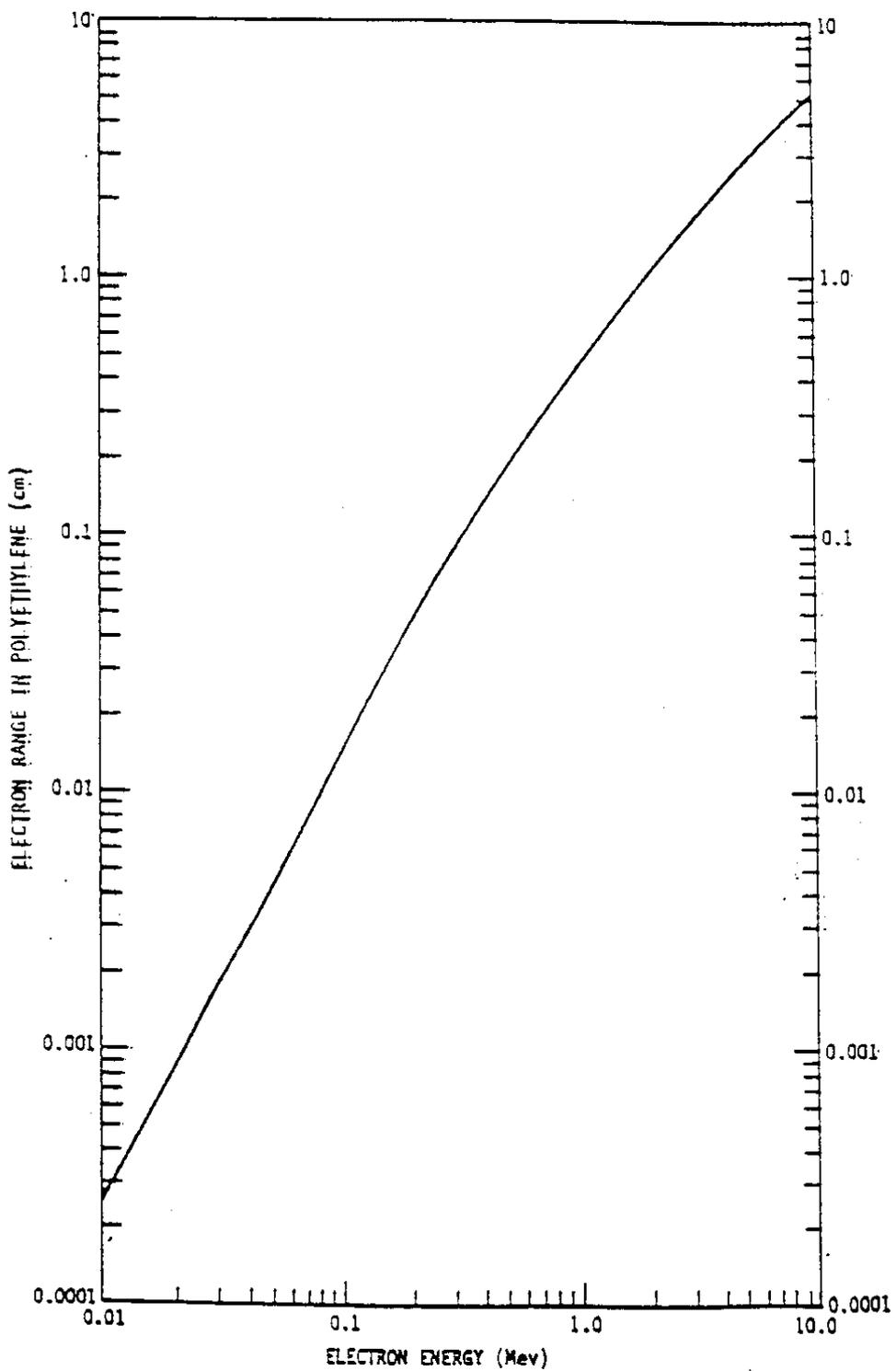
Figure 5

METEOSAT-P2 Space Environment Monitor
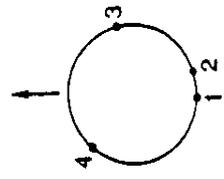
DAILY SUMMARY FOR DAY 179 (27 JUN) 1988

TIME (HRS UT)

Total Flux.

Flux.

Spectral Index

Polar Flow.

Azimuth.

Aniso-tropy

Axis

Kp

MUM

* $cm^{-2}sr^{-1}s^{-1}KeV^{-1}$

$Fig\ 6$

Meteosat P2, -18.3 deg

1987 -097, -38.4 deg

1982 -019, -165.1 deg

1984 -037, +69.0 deg

LT=01:07

LT=23:46

LT=15:19

LT=06:56

Injection event 02:20 UT
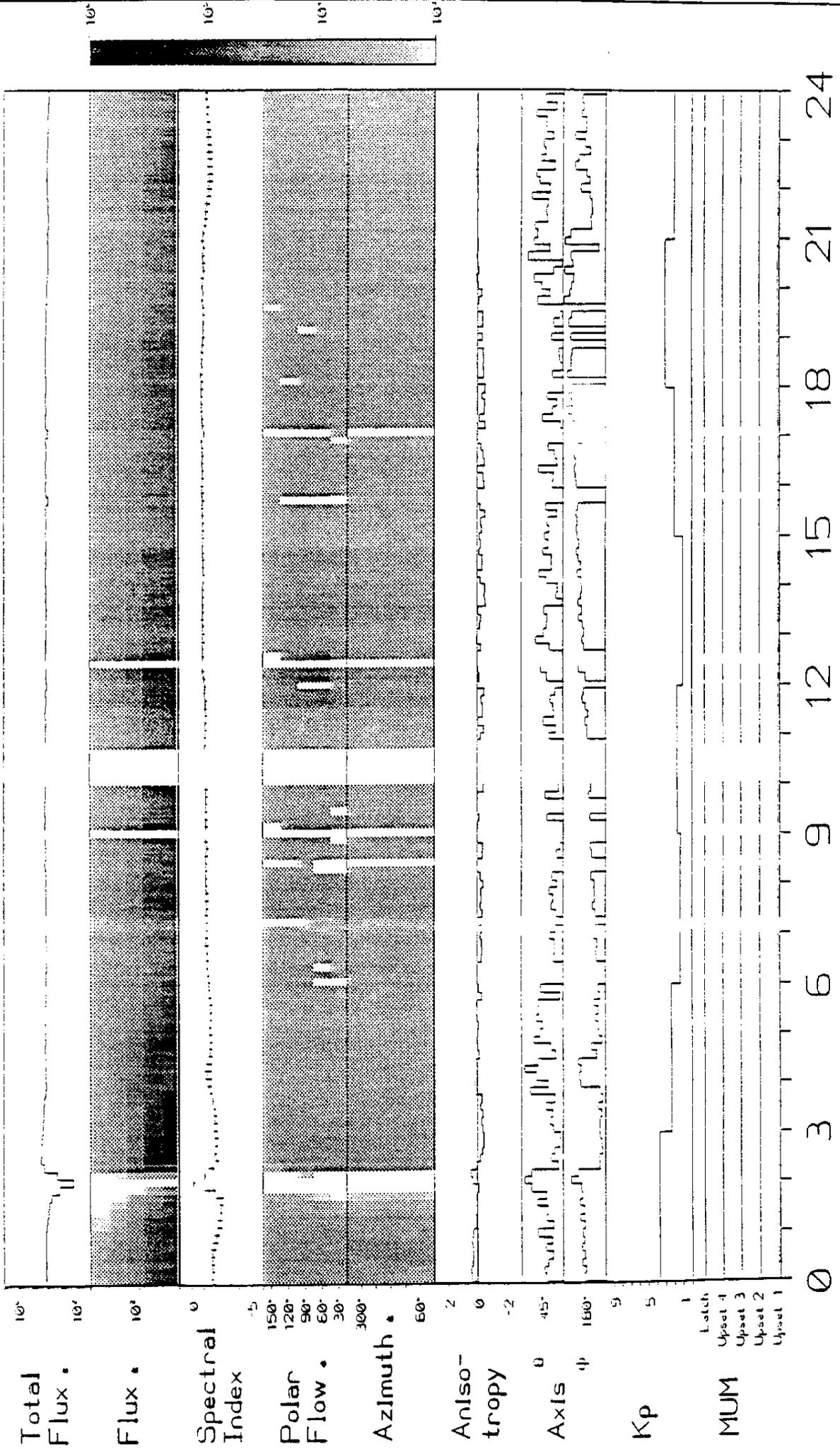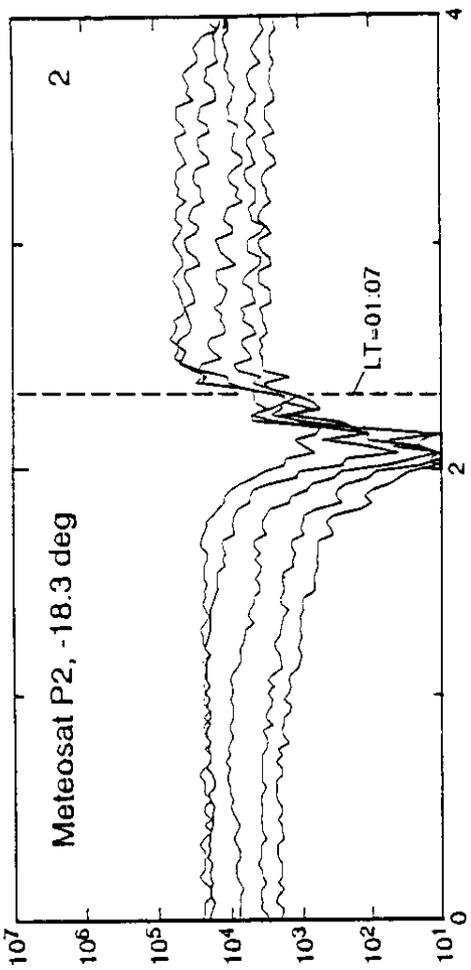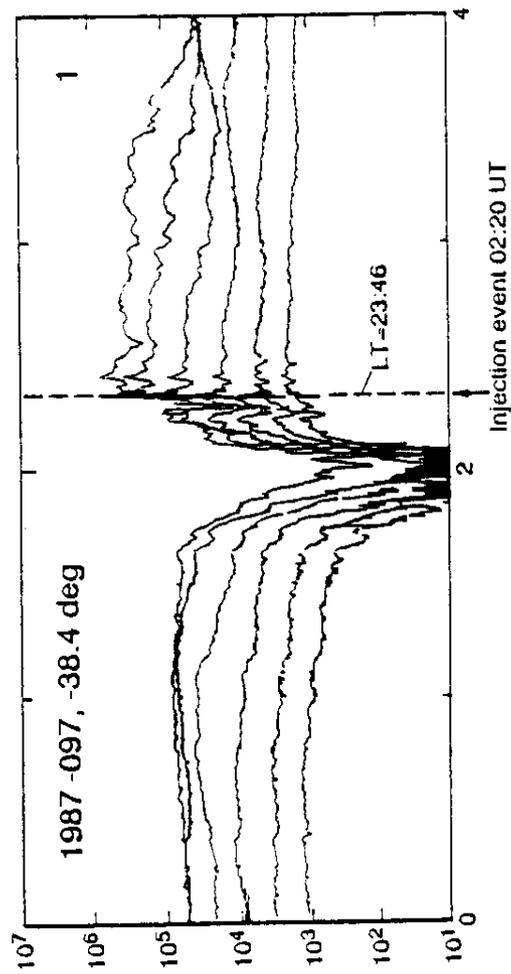
Sun at 02:20 UT

Time (UT)

27 JUNE, 1988

Flux (cm^-2 s^-1 keV^-1)

FIG 7

METEOSAT-P2 Space Environment Monitor

MONTHLY SUMMARY FOR MAR 1989

Total
Flux.

Flux.

Spectral
Index

Polar
Flow.

Azimuth.

Aniso-
tropy

Axis

Kp(τ)

MUM

1 3 5 7 9 11 13 15 17 19 21 23 25 27 29 31

DAY OF MONTH

* cm⁻²sr⁻¹s⁻¹KeV⁻¹

FG 8

Meteosat P2 anomalies: Jun 88–Jun 89

Month (1=Jan)

Local time (hours)

+ RPJ
✱ IRDS
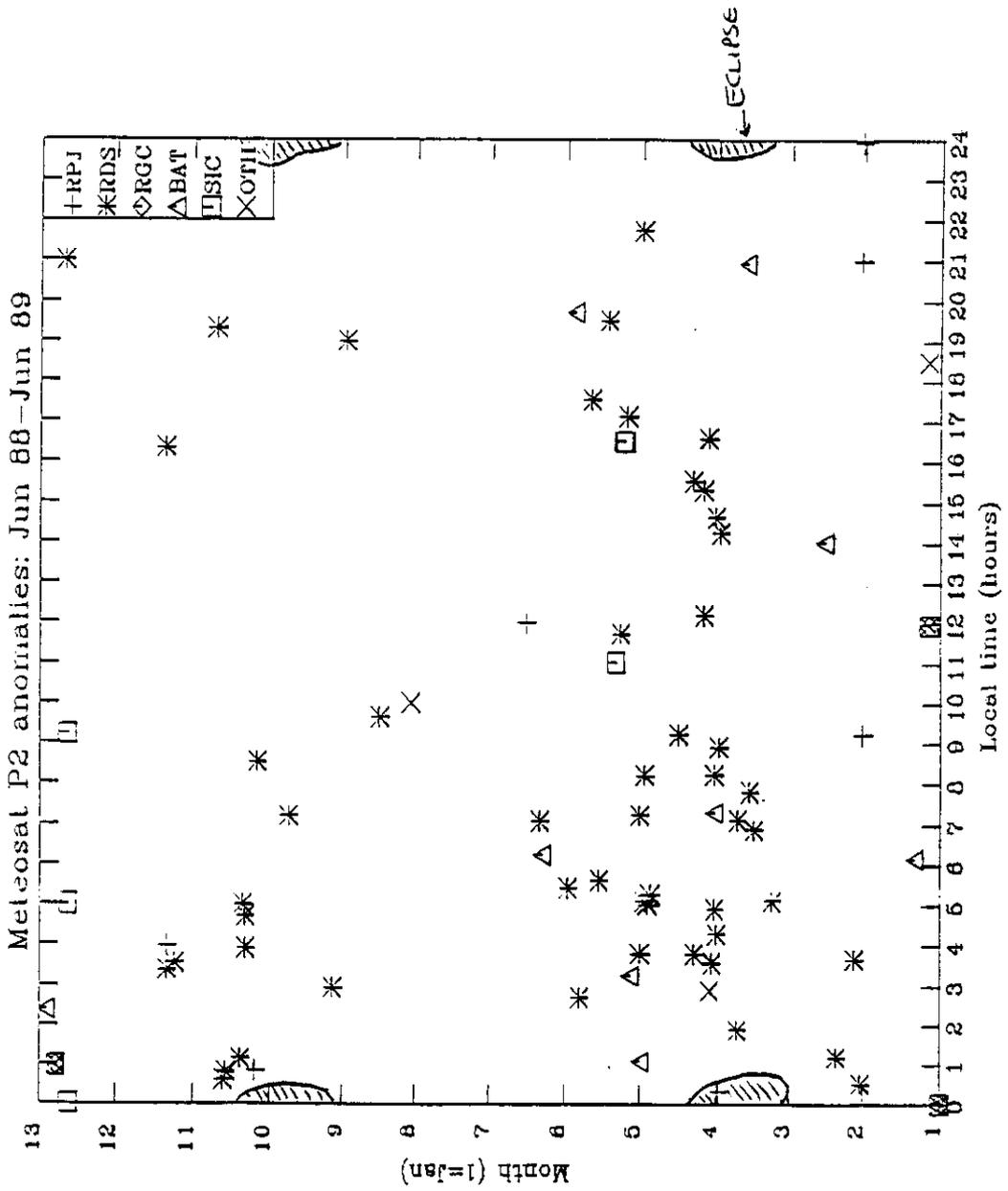◇ RGC
△ BAT
□ SIC
✕ OPH

ECLIPSE
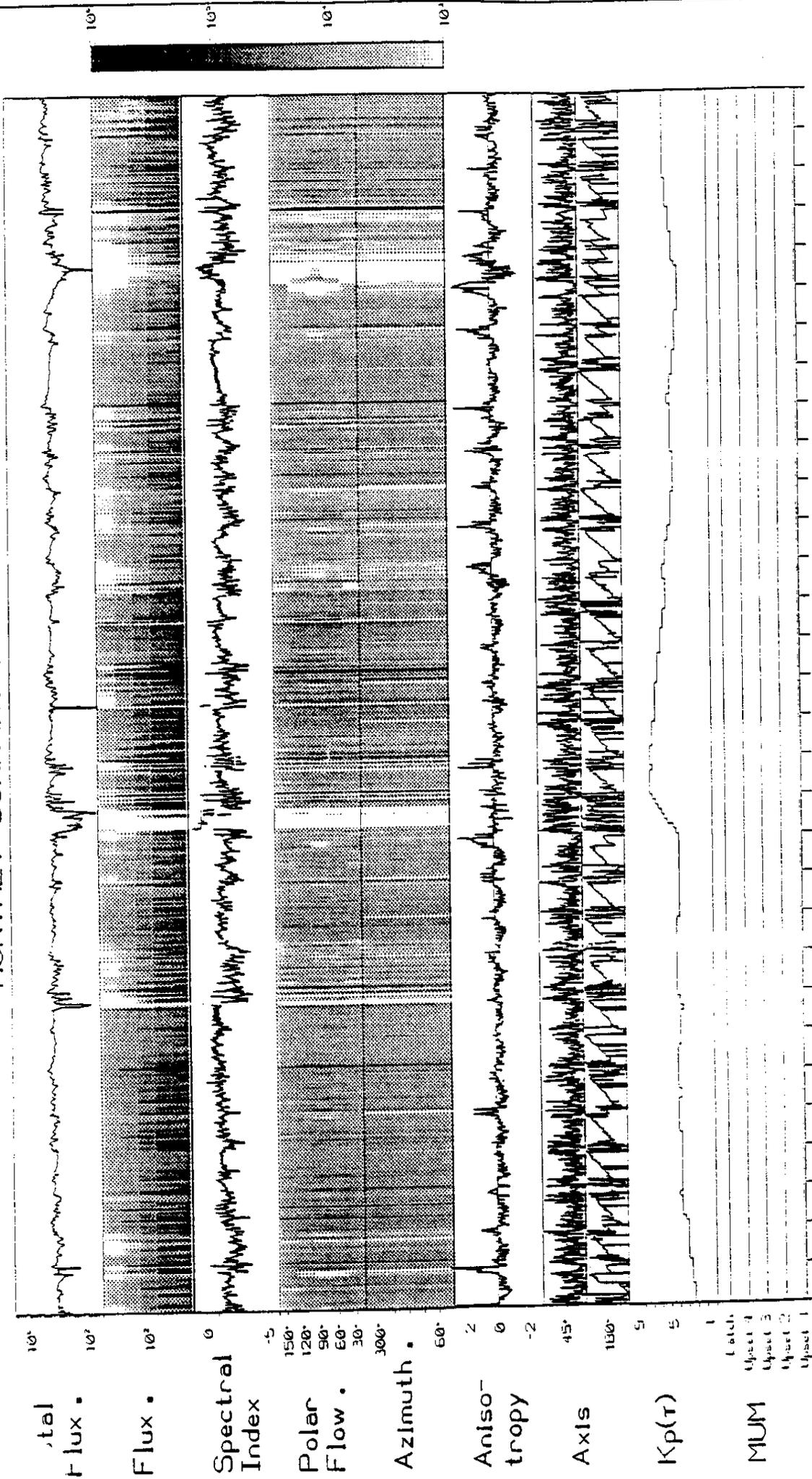
FIG 9

Plot Done 12-OCT-89 21:12:06
Frame 4 / 1 User A.K.

july 1988 to june 1989
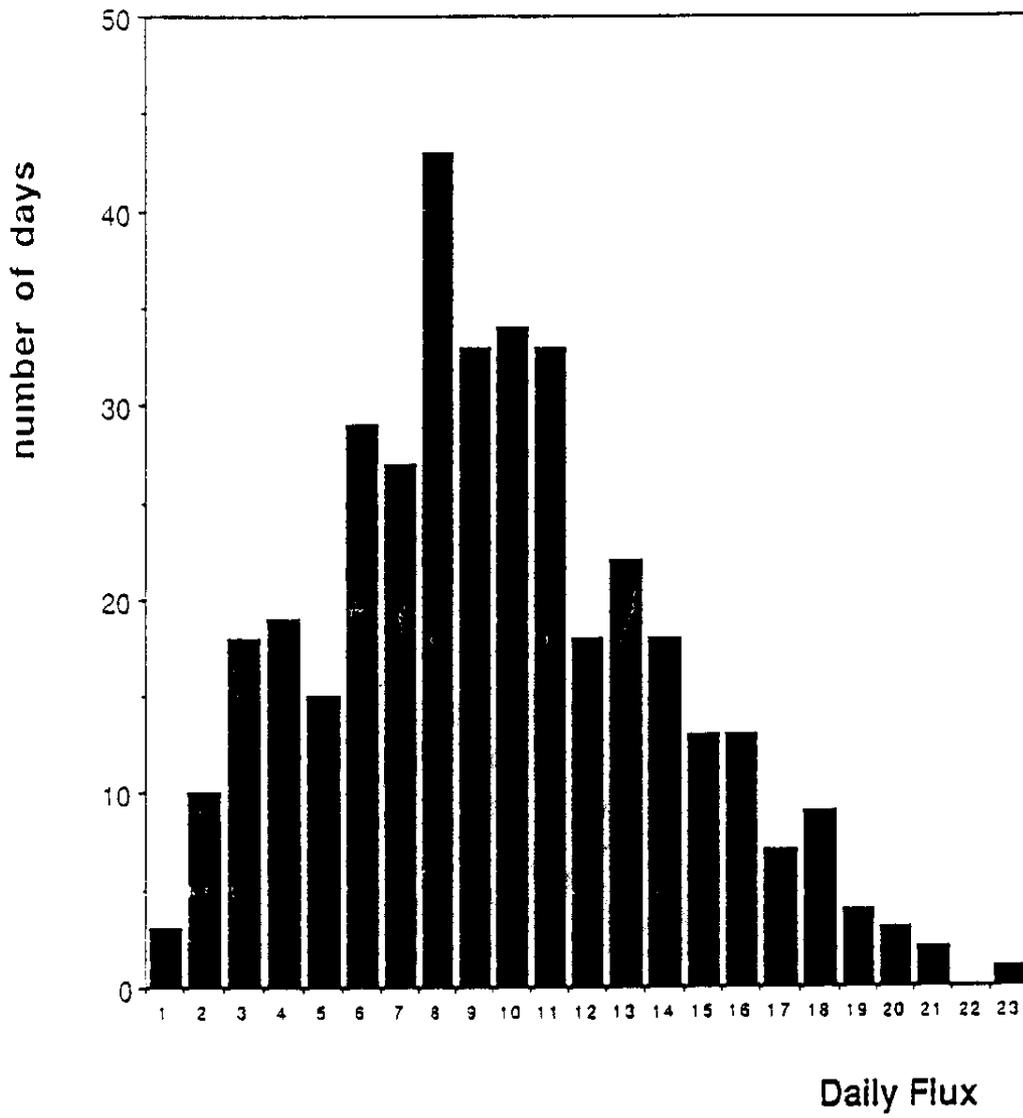
FIG 10

July 1988 to June 1989

Daily Flux
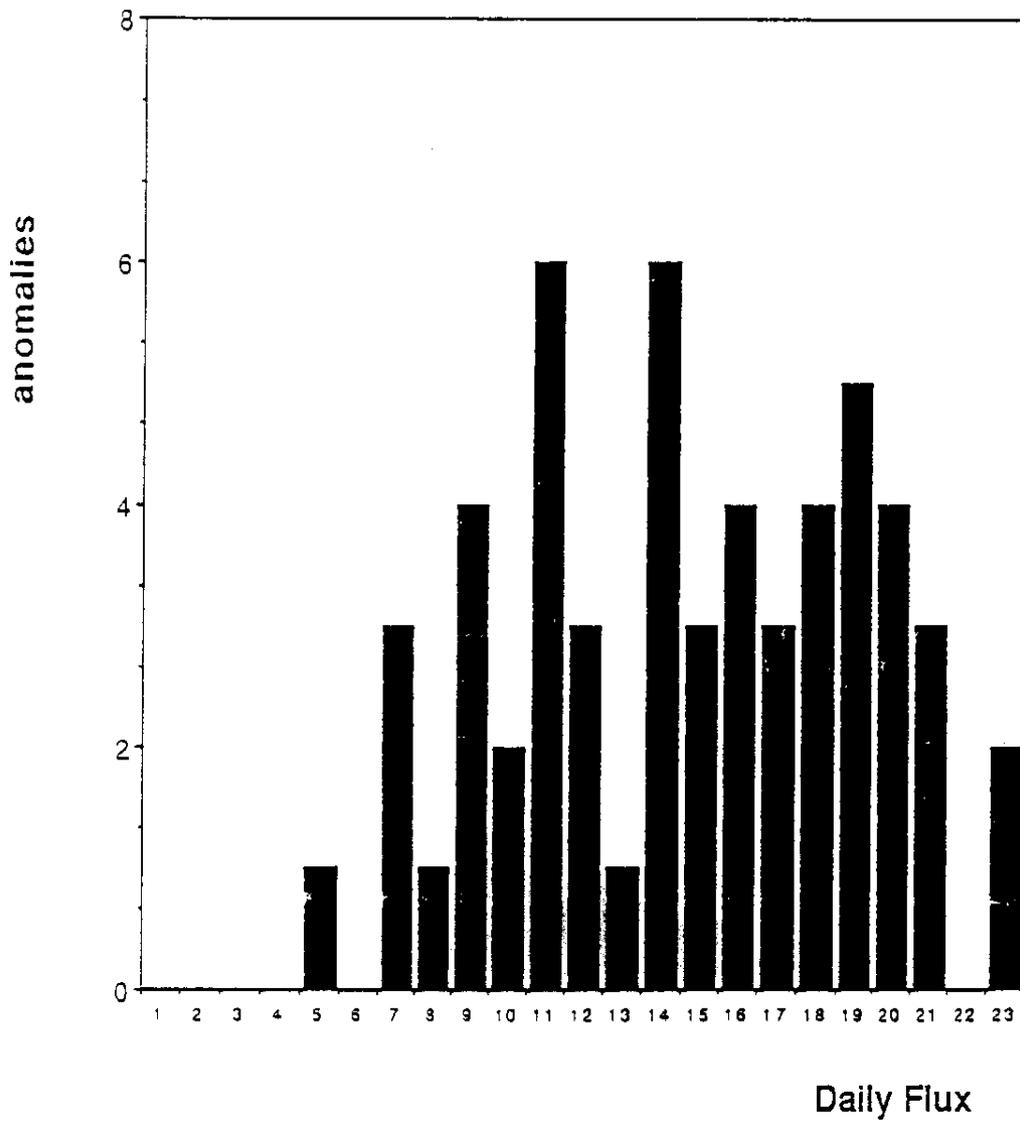
FIG 11

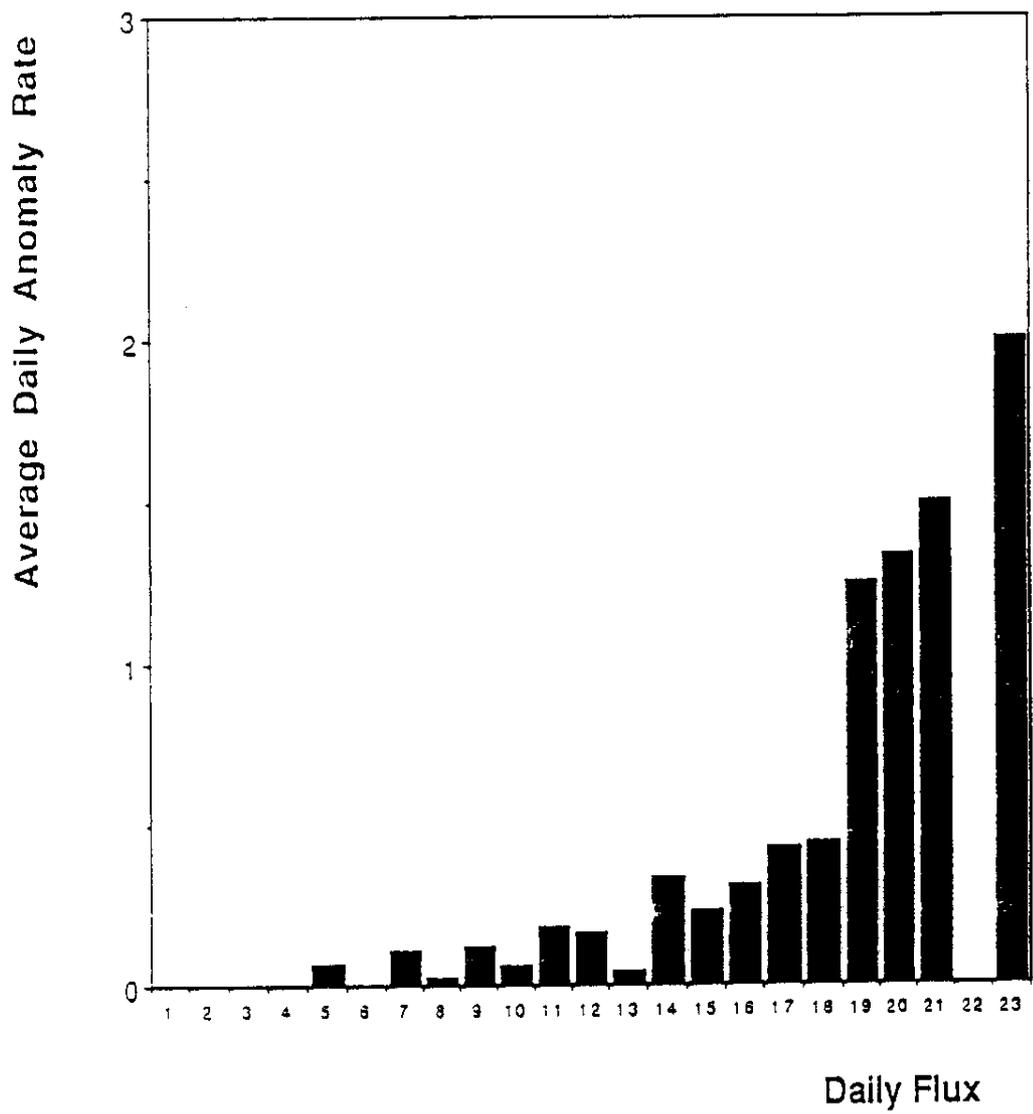# July 1988 to June 1989

FIG 12

July 1988 to June 1989

FIG 13

D-80282

FILE	INPUT RECS.	DATA RECORDS INPUT	LENGTH	MAX. SIZE	READ ERROR SUMMARY PERM	ZERO B	SHORT	UNDEF.	INPUT RETRIES #RECS.	TOTAL #
	1	2	5	1	80	2048 BYTES	0	0	0	0

FILE

0)	00000000	00000000	RECORD 00000000	1 00000000	AE46A86F	0D4756DD	CC47953F	2248E083	36481E61	BDC01BA2	523F67D6
4)	3848AD92	3848AD92	00000000	00000000	00000000	00000000	00000000	00000000	00000000	00000000	00000000
8)	00000000	00000000	00000000	00000000	00000000	00000000	00000000	00000000	00000000	00000000	00000000
12)	00000000	00000000	00000000	00000000	00000000	00000000	00000000	00000000	00000000	00000000	00000000
16)	00000000	00000000	00000000	00000000	00000000	00000000	00000000	00000000	00000000	00000000	00000000
20)	00000000	00000000	00000000	00000000	00000000	00000000	00000000	00000000	00000000	00000000	00000000
24)	00000000	00000000	00000000	00000000	00000000	00000000	00000000	00000000	00000000	00000000	00000000
28)	00000000	00000000	00000000	00000000	00000000	00000000	00000000	00000000	00000000	00000000	00000000
32)	00000000	00000000	00000000	00000000	00000000	00000000	00000000	00000000	00000000	00000000	00000000
36)	00000000	00000000	00000000	00000000	00000000	00000000	00000000	00000000	0F3FA52A	A447E9F1	8E465DD9
40)	2A476295	2A476295	E547FA62	5D48035E	8A488FE3	EAC0E358	3E3F1967	43489260	65483B97	5A4856C5	53486895
44)	3F489BC6	3F489BC6	00000000	00000000	00000000	00000000	00000000	00000000	00000000	00000000	00000000
48)	00000000	00000000	00000000	00000000	00000000	00000000	00000000	00000000	00000000	00000000	00000000
52)	00000000	00000000	00000000	00000000	00000000	00000000	00000000	00000000	00000000	00000000	00000000
56)	00000000	00000000	00000000	00000000	00000000	00000000	00000000	00000000	00000000	00000000	00000000
60)	00000000	00000000	00000000	00000000	00000000	00000000	00000000	00000000	00000000	00000000	00000000
64)	00000000	00000000	00000000	00000000	00000000	00000000	00000000	00000000	00000000	00000000	00000000
68)	00000000	00000000	00000000	00000000	00000000	00000000	00000000	00000000	00000000	00000000	00000000
72)	00000000	00000000	F8420000	0F3FA52A	9D3FB67B	AA47A777	BB461502	53471D11	24430000	80400000	30420000
76)	A8420000	A8420000	3F3FD08E	4F4871FB	72481A32	8C485D01	6E482398	F2477DA7	5648C078	7348282C
80)	C8C 9909	C8C 9909	00000000	00000000	00000000	00000000	CF486FFB	00000000	00000000	00000000	00000000
84)	00000000	00000000	00000000	00000000	00000000	00000000	00000000	00000000	00000000	00000000	00000000
88)	00000000	00000000	00000000	00000000	00000000	00000000	00000000	00000000	00000000	00000000	00000000
92)	00000000	00000000	00000000	00000000	00000000	00000000	00000000	00000000	00000000	00000000	00000000
96)	00000000	00000000	00000000	00000000	00000000	00000000	00000000	00000000	00000000	00000000	00000000
100)	00000000	00000000	00000000	00000000	00000000	00000000	00000000	00000000	00000000	00000000	00000000
104)	00000000	00000000	00000000	00000000	00000000	00000000	00000000	00000000	00000000	00000000	00000000
108)	00000000	00000000	00000000	00000000	00000000	00000000	00000000	00000000	00000000	00000000	00000000
112)	00000000	00000000	00000000	00000000	24440000	80410000	30430000	24430000	F8430000	9D3FB67B	E53FC911
116)	A2476610	A2476610	88465803	4B471548	ED471BC4	5948DE6E	6048867	D9C004C7	8A3FCE45	53486895	45488D2D
120)	53486895	53486895	00000000	5A4856C9	00000000	00000000	00000000	00000000	00000000	00000000	00000000
124)	00000000	00000000	00000000	00000000	00000000	00000000	00000000	00000000	00000000	00000000	00000000
128)	00000000	00000000	00000000	00000000	00000000	00000000	00000000	00000000	00000000	00000000	00000000
132)	00000000	00000000	00000000	00000000	00000000	00000000	00000000	00000000	00000000	00000000	00000000
136)	00000000	00000000	00000000	00000000	00000000	00000000	00000000	00000000	00000000	00000000	00000000
140)	00000000	00000000	00000000	00000000	00000000	00000000	00000000	00000000	00000000	00000000	00000000
144)	00000000	00000000	00000000	00000000	00000000	00000000	00000000	00000000	00000000	00000000	00000000
148)	00000000	00000000	00000000	00000000	00000000	00000000	00000000	00000000	00000000	00000000	76440000
152)	C0410000	C0410000	84430000	FC430000	3A440000	E53FC811	15402E53	9C47414D	6F465305	38473F40	F84798C3
156)	5648C078	5648C078	4A482D05	DEC01F73	A83F8018	55486462	484883C7	3348BA2B	53486895	65483B97	00000000
160)	00000000	00000000	00000000	00000000	00000000	00000000	00000000	00000000	00000000	00000000	00000000
164)	00000000	00000000	00000000	00000000	00000000	00000000	00000000	00000000	00000000	00000000	00000000
168)	00000000	00000000	00000000	00000000	00000000	00000000	00000000	00000000	00000000	00000000	00000000
172)	00000000	00000000	00000000	00000000	00000000	00000000	00000000	00000000	00000000	00000000	00000000
176)	00000000	00000000	00000000	00000000	00000000	00000000	00000000	00000000	00000000	00000000	00000000
180)	00000000	00000000	00000000	00000000	00000000	00000000	00000000	00000000	00000000	00000000	00000000
184)	00000000	00000000	00000000	00000000	00000000	00000000	00000000	00000000	00000000	00000000	00000000
188)	00000000	00000000	00000000	00000000	4D440000	00000000	A0410000	A0410000	5C430000	D2430000	1B440000
192)	5E5E5E5E	5E5E5E5E	5E5E5E5E	5E5E5E5E	5E5E5E5E	5E5E5E5E	5E5E5E5E	5E5E5E5E	5E5E5E5E	5E5E5E5E	5E5E5E5E
196)	5E5E5E5E	5E5E5E5E	5E5E5E5E	5E5E5E5E	5E5E5E5E	5E5E5E5E	5E5E5E5E	5E5E5E5E	5E5E5E5E	5E5E5E5E	5E5E5E5E
200)	5E5E5E5E	5E5E5E5E	5E5E5E5E	5E5E5E5E	5E5E5E5E	5E5E5E5E	5E5E5E5E	5E5E5E5E	5E5E5E5E	5E5E5E5E	5E5E5E5E
204)	5E5E5E5E	5E5E5E5E	5E5E5E5E	5E5E5E5E	5E5E5E5E	5E5E5E5E	5E5E5E5E	5E5E5E5E	5E5E5E5E	5E5E5E5E	5E5E5E5E

FILE INPUT DATA RECORDS MAX. READ ERROR SUMMARY INPUT RETRIES

```
              RECS.        INPUT           #RECS.    TOTAL#
           2    962         962                0         0

FILE   89  RECORD    INPUT  LENGTH  SIZE   PERM  ZERO B  SHORT  UNDEF.  #RECS.  TOTAL#
                             289            2048 384BYTES
( 0)       00000000  00000000 00000000 00000000 00000000 00000000 00000000 00000000 00000000
( 40)      00000000  00000000 00000000 00000000 00000000 00000000 00000000 00000000 00000000
( 80)      00000000  00000000 00000000 00000000 00000000 00000000 00000000 00000000 00000000
(120)      00000000  00000000 00000000 00000000 00000000 00000000 00000000 00000000 00000000
(160)      00000000  00000000 00000000 00000000 00000000 00000000 00000000 00000000 00000000
(200)      00000000  00000000 00000000 00000000 00000000 00000000 00000000 00000000 00000000
(240)      00000000  00000000 00000000 00000000 00000000 00000000 00000000 00000000 00000000
(280)      00000000  00000000 00000000 00000000 00000000 00000000 00000000 00000000 00000000
(320)      00000000  00000000 00000000 00000000 00000000 00000000 00000000 00000000 00000000
(360)      00000000  00000000 00000000 00000000 00000000 00000000 00000000 00000000 00000000

FILE  INPUT   DATA RECORDS   MAX.        READ ERROR SUMMARY        INPUT RETRIES
      RECS.   INPUT          SIZE   PERM  ZERO B  SHORT  UNDEF.   #RECS.   TOTAL#
  89    289      290         2048     0     0      0       0         0        0

EOJ       DUMP STOPPED AFTER FILE   9       # OF PERMANENT READ ERRORS   0

START TIME  9/22/90  11:13:09      STOP TIME  09/22/90  11:17:41

$$
$EXE TPJUMP BS
```

INPUT TAPE   JROUTC2 ON HT1
DATA INPUT   H9 NF=90 SR=2=LAST=1 SR=89=1 1

FILE	INPUT RECS.	DATA RECORDS INPUT		MAX. SIZE		READ ERROR SUMMARY PERM ZERO B	SHORT	UNDEF.		INPUT RETRIES #RECS.	TOTAL#
1	5	962	LENGTH	80	384BYTES	0	0	0	0	0	0

FILE 2 RECORD   962 LENGTH   384BYTES

0)	334589E1	334545EC	3A47D412	0047B713	ED462898	3947A80B	B1476977E	B1476977E	75C0E85D	363F69B7
4)	0E489841	1F48EC5C	F34716FF	1B48F6C2	93484B35	BC46EDDF	C34621C7	B746A6C6	B4467327	B746C64F
8)	C446BEE1	81467700	A4466066	C346C570	D0466876	D246E6AE	CA462619	D346EF18	0447F90F	BD462013
12)	BD462013	BD46893D	D246E9AE	B2463B45	A14634B	8A465686	B2463845	A2461AE9	8E465E4F	B7464282
16)	B74619CA	C846DC1C	D246E9AE	D246E9AE	C7462EA5	F2463845	CD46F847	C34628BA	64466D8E	8F46690A
20)	E54612AC	00000000	00000000	00000000	00000000	00000000	00000000	00000000	00000000	00000000
24)	00000000	00000000	00000000	00000000	00000000	00000000	00000000	00000000	00000000	00000000
28)	00000000	00000000	00000000	00000000	00000000	00000000	00000000	00000000	00000000	00000000
32)	00000000	00000000	00000000	00000000	00000000	00000000	00000000	00000000	00000000	00000000
36)	E144608C	30420200	F2430900	AA449080	67440000	F2430000	963ED6F1	2A43BD23	52449076	00000000

FILE	INPUT RECS.	DATA RECORDS INPUT		MAX. SIZE		READ ERROR SUMMARY PERM ZERO B	SHORT	UNDEF.		INPUT RETRIES #RECS.	TOTAL#
2	962	963	LENGTH	1	2048	0	0	0	0	0	0

FILE 89 RECORD   1 LENGTH   2048BYTES

0)	00000000	00400000	A14625E6	7A450000	DB45BACD	D3468180	80470A67	97472B0C	05C128FB	783F5663
4)	7E471D21	4B47FC7A	F34716FF	37472FAC	86473BB7	FD4531A6	FF45398S	09460FF7	F7453B13	F7452IC8
8)	0246BD19	B7459B52	26460C7	404629C6	3846COFB	09466C06	A6453EC9	B545E878	EC450663	35460DD0C
12)	2E46C2E1	09460AD8	E3455562	B34555EC	8D45C85F	E1453CDC	B045FFD5	9D45A25D	C345FAB0	22461173
16)	FA45D920	D045261B	93455286	D745C4B1	28463536	47466B50	1E462C8C	C645EE10	B945D018	1E462A0E
20)	3846315C	00000000	00000000	00000000	00000000	00000000	00000000	00000000	00000000	00000000
24)	00000000	00000000	00000000	00000000	00000000	00000000	00000000	00000000	00000000	00000000
28)	00000000	00000000	00000000	00000000	00000000	00000000	1D4051C6	CD42A5EC	384429F8	00000000
32)	00000000	2444E9EB	80410500	30430000	A8430000	F8430000	04400000	80400000	A0452C39	7A450000
36)	B245A82F	8546F9EB	7A4747C0	DC473014	14C1CAB9	633F170B	37475B5F	2C477591	C2463F2D	2D47C8C4
40)	84470EA7	EA45D80C	E945415A	F245FC19	E445A4AE	E4451D7	ED451C38	BA4537A2	20460510	2846B0F6
44)	2746B8C5	D54575EA	8C45C1DB	9745DCAD	C845A4AE	1B467D3A	2046EA88	054637I0	B1459F06	8A451BA7
48)	984554F1	AA455E06	98450700	A7452307	A345ACDD	C4452578	A9453AC5	99459143	EA452850	00000000
52)	414665BA	374678F8	14460B37	DE45F853	B545E94A	03468B62	1E460871	00000000	00000000	00000000
56)	00000000	00000000	00000000	00000000	00000000	00000000	00000000	00000000	00000000	00000000
60)	00000000	00000000	00000000	00000000	00000000	00000000	00000000	00000000	00000000	00000000
64)	00000000	1146BB0	92425D6E	32442C62	00000000	5A44ABAA	5A44ABAA	AA41ABAA	6A43ABAA	6A43ABAA
68)	E6430000	8041000	C0400000	C146E90A	7A450000	AE4674E0	CE45F588	AA41ABAA	9C47C0BE	1E489E87
72)	21C156CD	5247BFFB	80476573	1347B75B	554763C2	90473CA8	0F46E570	0345CE82	14461CC4
76)	12461EC6	0C466F35	1346A586	EA4563A7	204653C8	2D466100	0E46293D	014668F8	0746CC59
80)	1946A44E	51469BEC	4946035	1A46EA34	0D462FCC	D74537B3	F44585B3	DA4535D3	CC45155D
84)	0945540B	30463C3	FC45D332	F545677E	EC45C082	0F46=97B	41465F8E	1846BF37	0745B32E
88)	034637E6	1E4691EE	23461BCA	00000000	00000000	00000000	34462D23	1846289	00000000
92)	00000000	00000000	00000000	00000000	00000000	00000000	00000000	024658995	00000000
96)	00000000	00000000	00000000	00000000	00000000	00000000	00000000	0D46C2C5	8F3F453C	DD42F364
100)	00000000	00000000	00000000	00000000	00000000	00000000	00000000	00000000	00000000	00410000
104)	E6430000	254455555	2BC1E3F9	C0400000	254455555	E6430000	EQ430000	C040000	7947A89F
108)	E5464015	7A450000	A7456C51	3948AF50	AD477355	6A43ABAA	2BC1E3F9	4C4718B	0346EA15
112)	2E443C4B	7A45000	7E471E20	B4463281	1F45EA46	3948AF50	E0430000	8C3F4362	7947A89F
116)	E5464015	52474D63	A7456C51	18462793	194659F0	1F45EA46	2BC1E3F9	1B468367	0346EA15
120)	4C477B61	1046A2A9	7E471E20	19464B00	07467FDF	22465CF5	14460FA6	17464555	1E4616C4
124)	15460C4	124674J1	15467D45	11468DE8	1646F4AD	12465CF5	22464763	2C468A2E	1A46350
128)	2246E52	1E46120A	11468DE8	2B462620	164600C	1646F4AD	14460A90	454648DA	1A46350
132)	1046F06E	00000000	2B462620	27468329	18468E7C	15463102	0246A5995	1846289	00000000
136)	00000000	00000000	00000000	00000000	00000000	00000000	024658995	1846B8F37	00000000
140)	00000000	00000000	00000000	00000000	00000000	00000000	00000000	0D46C2C5	00000000
144)	00000000	00000000	00000000	8E3E0202	3443B8CA	3E44D405	00000000	3E44D405	61440080

```
( 1520)  B0410000 72430000 E7430000 2A440080 00410000 20410000 20410000 2F47D03F 7A450000 0F462B75 1E4716CF
( 1560)  14483B38 73481054 35C1F657 463F7829 C9472D61 C047EDF9 99479DCF AC477591 C84784C7 65460B98
( 1600)  5E463579 6546CF37 5546578C 6A46710C 6D46AB4F 3C46CF51 66465C76 87465700 8145539F AF46E72B
( 1640)  83469B92 6C461DF1 7446A784 9A4661E7 8846413B 8D46B5FE 87460307 4346E5D7 43463033 4D46BF7D
( 1680)  42468AF2 38462009 42467318 94465296 4D46CB60 49466C30 4D46CB60 414681F9 37466396 65468BB0
( 1720)  6C4603FF 2546698C 14468512 2C46770B 774633C1 00000000 00000000 00000000 00000000 00000000
( 1760)  00000000 00000000 00000000 00000000 00000000 00000000 00000000 00000000 00000000 00000000
( 1800)  00000000 00000000 00000000 00000000 00000000 00000000 00000000 00000000 00000000 00000000
( 1840)  00000000 00000000 00000000 00000000 5A444ABAA AA41ABAA A643ABAA 6A43ABAA E043000 25445555
( 1880)  573F60EC C142F60B 5B447CB9 00000000 5A444ABAA 5E5E5E5E 5E5E5E5E 5E5E5E5E 5E5E5E5E 5E5E5E5E
( 1920)  5E5E5E5E 5E5E5E5E 5E5E5E5E 5E5E5E5E 5E5E5E5E 5E5E5E5E 5E5E5E5E 5E5E5E5E 5E5E5E5E 5E5E5E5E
( 1960)  5E5E5E5E 5E5E5E5E 5E5E5E5E 5E5E5E5E 5E5E5E5E 5E5E5E5E 5E5E5E5E 5E5E5E5E 5E5E5E5E 5E5E5E5E
( 2000)  5E5E5E5E 5E5E5E5E 5E5E5E5E 5E5E5E5E 5E5E5E5E 5E5E5E5E 5E5E5E5E 5E5E5E5E 5E5E5E5E 5E5E5E5E
( 2040)  5E5E5E5E 5E5E5E5E 5E5E5E5E 5E5E5E5E 5E5E5E5E 5E5E5E5E 5E5E5E5E 5E5E5E5E 5E5E5E5E 5E5E5E5E
```

```
FILE   INPUT   DATA RECORDS   MAX.         READ ERROR SUMMARY         INPUT RETRIES
       RECS.     INPUT        SIZE    PERM ZERO B SHORT UNDEF.   #RECS.  TOTAL#
  89    289       289         2048     0     0     0     0    0     0       0

EOJ     DUMP STOPPED AFTER FILE   90        # OF PERMANENT READ ERRORS  0

START TIME 09/22/90  11:18:52       STOP TIME 09/22/90  11:22:41
```

$$